Electron transfer of functionalized quinones in acetonitrile

Tzu-Yao Hsu, Roxanne Berthin, Alessandra Serva, Kyle Reeves, Mathieu Salanne, Guillaume Jeanmairet

Electron Transfer of Functionalised Quinones in Acetonitrile

Tzu-Yao Hsu,[1,2] Roxanne Berthin,[1,2] Alessandra Serva,[1,2] Kyle Reeves,[3] Mathieu Salanne,[1,2,4,a)] and Guillaume Jeanmairet[1,2,b)]

[1)] *Sorbonne Université, CNRS, Physico-Chimie des Électrolytes et Nanosystèmes Interfaciaux, PHENIX, F-75005 Paris, France*

[2)] *Réseau sur le Stockage Électrochimique de l'Énergie (RS2E), FR CNRS 3459, 80039 Amiens Cedex, France*

[3)] *Maison de la Simulation, CEA, CNRS, Univ. Paris-Sud, UVSQ, Université Paris-Saclay, 91191 Gif-sur-Yvette, France*

[4)] *Institut Universitaire de France (IUF), 75231 Paris, France*

(Dated: 8 June 2022)

Quinones are redox active organic molecules that have been proposed as an alternative choice to metal-based materials in electrochemical energy storage devices. Functionalization allows to fine tune not only their chemical stability but also the redox potential and the kinetics of the electron transfer reaction. However, reaction rate constant is not solely determined by the redox species but is also impacted by solvent effects. In this work, we show how the functionalization of benzoquinone with different functional groups impacts the solvent reorganization free energies of electron transfer half-reactions in acetonitrile. The use of molecular density functional theory, whose computational cost for studying electron transfer reaction is considerably reduced compared to state-of-the art molecular dynamics simulations, enables to perform a systematic study. We validate the method by comparing the predictions of the solvation shell structure and the free energy profiles for electron transfer reaction to reference classical molecular dynamics simulations in the case of anthraquinone solvated in acetonitrile. We show that all the studied electron transfer half-reactions follow Marcus' description, regardless of functional groups. Consequently, the solvent reorganization free energy decreases as the molecular size increases.

I. INTRODUCTION

Quinones are a family of organic molecules that can undergo reversible redox reactions[1–6]. The capability of carrying electrons allows them to play an important role in biological processes such as oxygenic photosynthesis and aerobatic respiratory chain[7–10]. They have also been proposed as promising candidates for energy storage applications, in particular for organic redox-flow batteries[11–18]. Such devices would be highly suitable for stationary storage since they do not use metallic elements prone to supply risks (such as cobalt) and the reactive species are stored in separate tanks, allowing for much longer-term storage than conventional devices such as Li-ion batteries.

A main advantage of such organic molecules is the versatility of their molecular structure. It allows chemists to tune their chemical properties according to the desired application. Much effort has been made to understand the effect of modifying molecular structure on the redox potential[2,19,20] and the possible irreversible side reactions[21–23]. For redox-flow battery applications, understanding how functionalization affects the redox properties can help to improve the energy density, that is the amount of energy stored per unit volume and the cycle-life of the devices. However, reports discussing reaction kinetics of functionalized quinones, that is related to the amount of power a device can deliver, remain very scarce.[4,5,24–27]. In particular, the impact of solvent effect on kinetics is often disregarded.

From a theoretical point of view, Marcus theory is a widely accepted model of electron transfer reactions (ETR) that can serve as a good starting point for studying redox reaction kinetics in solution[28–36]. When the electronic coupling of oxidised and reduced states is weak, the electron transfer occurs at the transition state which corresponds to a set of solvent configurations in which the reduced and the oxidized state have the same energy. Using macroscopic electrostatics, Marcus derived a relation linking the activation free energy to the reaction free energy and the solvent reorganization free energy, often denoted λ. This quantity measures the free energy cost to reorganize the solvent molecules around the reactant to a configuration that would be in equilibrium with the product.

Molecular dynamics has long been the method of choice to investigate the influence of molecular effects on ETR that are ignored by Marcus macroscopic description. A few reports have applied these methods to study quinones[37–39]. Vandevondele *et al.* generated trajectories of benzoquinone (BQ) and duroquinone (DQ) solvated in acetonitrile using classical molecular dynamics (MD). They then computed the energy cost to reduce the molecule using electronic density functional theory before evaluating the exponential part of reaction rate constant[37]. Reeves *et al.* simulated anthraquinone (AQ) and ionic liquid grafted with anthraquinone solvated in acetonitrile using ab-initio molecular dynamics (AIMD)[38]. They reported the free energy profiles computed with simulation

[a)] Electronic mail: mathieu.salanne@sorbonne-universite.fr
[b)] Electronic mail: guillaume.jeanmairet@sorbonne-universite.fr

which could not be interpreted by Marcus theory but required the use of a two-Gaussian states model[40] instead. However, because the associated solvent configurations have a low probability, it is a tedious task to properly sample the region close to the transition state which makes the construction of free energy profiles computationally demanding. We recently proposed an alternative approach based on molecular density functional theory (MDFT) which is based on functional minimisation rather than on statistical sampling, and thus considerably reduces the computational cost as compared to MD[41,42].

In this work, we start by computing the solvation structure and the free energy profiles of AQ and its reduced anion (AQ^-) in acetonitrile (MeCN) using MD simulations and a recently developed polarizable force field[43]. This serves as a benchmark for MDFT calculations using generic force fields. The results show that MDFT provides a solvation structure in good agreement with classical MD simulations as well as a good estimate of the solvent reorganization free energies. The free energy profiles of one electron transfer half-reactions of BQ and DQ and their reduced anions, BQ^- and DQ^-, solvated in MeCN are then computed using MDFT. Finally, we carry a systematic study of solvent reorganization free energies for several functionalized BQ derivatives modeled with a generic force field using MDFT.

II. THEORY

A. Marcus theory

Let's consider a half-cell reduction reaction

$$\mathrm{Ox} + e^- = \mathrm{Red} \tag{1}$$

where Ox and Red stand for oxidised and reduced state, respectively. Based on a transition-state formalism[44–48], the rate constant of the ETR, k, can be written as

$$k = A \exp\left(-\frac{\Delta G^\ddagger}{k_B T}\right) \tag{2}$$

where A is a pre-exponential factor that depends on the nature of the redox couple and of the solvent, $\Delta G^\ddagger$ is the activation free energy, k_B is the Boltzmann constant, and T is the temperature. Although it is difficult to predict the absolute values of the standard rate constant from simulation, one can easily compare the activation free energy of two reactions to estimate the ratio of their kinetic constants. This assumes that the pre-exponential factor A of Equation 2 is similar for a series of molecules having similar chemical structures which seems a reasonable hypothesis. $\Delta G^\ddagger$ can be further separated into inner-sphere and outer-sphere contributions

$$\Delta G^\ddagger = \Delta G^\ddagger_{\mathrm{is}} + \Delta G^\ddagger_{\mathrm{os}}. \tag{3}$$

The inner-sphere part, $\Delta G^\ddagger_{\mathrm{is}}$, involves intramolecular change as well as electronic structure rearrangement of the reactant to reach the transition state. The outer-sphere part, $\Delta G^\ddagger_{\mathrm{os}}$, is due to rearrangement of solvent molecules surrounding the solute. In the scope of this paper, we will only focus on the outer-sphere contribution. Note that the determination of $\Delta G^\ddagger_{\mathrm{is}}$ would require quantum chemistry calculations.

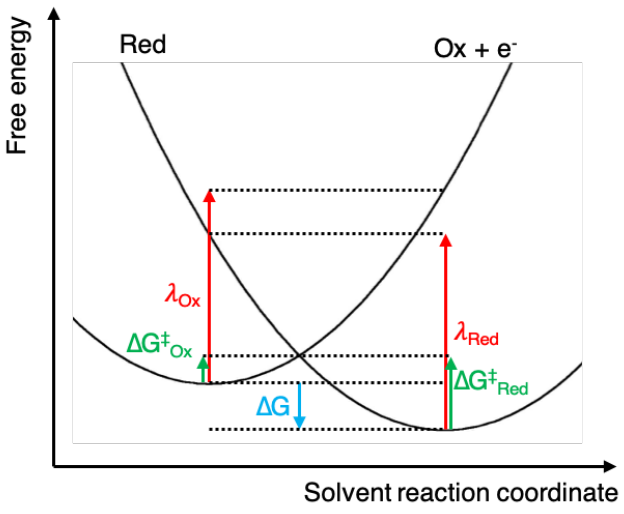

FIG. 1. Schematic representation of free energy profile as a function of a solvent reaction coordinate.

Marcus proposed a theoretical framework to estimate the activation free energy that is connected to the rate constant through Equation 2. This theory allows to compute the free energy of the oxidized and reduced states as a function of a solvent reaction coordinate. Such free energy profiles are schematically represented on Figure 1 where several quantities that are useful to characterize ETR, in particular the solvent reorganization free energies, λ_{Ox} and λ_{Red}, are displayed. λ_{Ox} (λ_{Red}) measures the free energy cost to rearrange the solvent molecules around the oxidized (reduced) state until they reach a configuration that would be in equilibrium with the reduced (oxidized) state.

Assuming a linear response of the solvent polarization to a change of electric charge of the solute, Marcus was able to show that the free energy of the reduced and oxidized states depend quadratically on the solvent reaction coordinate. As a result, both free energy profiles displayed on Figure 1 would be parabolic. Moreover, the curvature of the parabola for each are connected to the corresponding reorganization free energy λ. Within Marcus assumption $\lambda_{\mathrm{Ox}} = \lambda_{\mathrm{Red}}$ and the parabolas have identical curvature.

The activation free energy depends on the reaction free energy and the reorganization free energy through

$$\Delta G^\ddagger_{\mathrm{os}} = \frac{(\lambda + \Delta G)^2}{4\lambda}. \tag{4}$$

In an electrochemical experiment, ΔG can be tuned by changing the electrode potential, and equation 4 reduces

to $\Delta G^{\ddagger}_{\rm os} = \lambda/4$ when $\Delta G = 0$.

Marcus also proposed an analytical approximation for λ in the case of a spherical solute of radius r[33]

$$\lambda = \frac{e^2}{8\pi\epsilon_0 r}\left(\frac{1}{\epsilon_{\rm op}} - \frac{1}{\epsilon_{\rm s}}\right) \tag{5}$$

where e is the elementary charge, ϵ_0 is the vacuum permittivity, ϵ_{op} and ϵ_s are respectively the optical and static dielectric permittivity of solvent. Besides its evident success, Marcus theory is based on macroscopic electrostatics and does not account for effects occurring at the molecular scale. A good way to account for such effects is to resort to molecular simulations, such as MD.

B. Modelling Electron transfer using classical MD

To compute free energy profiles as displayed on Figure 1 using MD it is essential to define an appropriate solvent reaction coordinate. Warshel introduced the so-called vertical energy gap (VEG)[49], a choice that has been widely adopted since then. The VEG, ΔE, is defined as the difference between the reduced and oxidized state energies for a given solvent configuration

$$\Delta E(\boldsymbol{R}^N) = E_{\rm Red}(\boldsymbol{R}^N) - E_{\rm Ox}(\boldsymbol{R}^N) \tag{6}$$

where $\boldsymbol{R}^N$ denotes the position of all atoms. In practice, a set of atomic configurations $\boldsymbol{R}^N$ is generated by a MD simulation of the reduced state. The reduced energies $E_{\rm Red}(\boldsymbol{R}^N)$ are computed during the MD run. The energy of the oxidized state, $E_{\rm Ox}(\boldsymbol{R}^N)$, can either be computed on the fly during the simulation or as a post-processing step by reading the stored atomic configurations. The probability distribution of the VEG for the reduced state, $P_{\rm Red}(\Delta E)$, can then be computed through histogramming. The same procedure is followed to compute the probability distribution of the VEG for the oxidized state, $P_{\rm Ox}(\Delta E)$.

It is then possible to compute the free energy as a function of the reaction coordinate

$$G_A(\Delta E) = -k_B T \ln(P_A(\Delta E)) + \bar{G}_A \tag{7}$$

where A stands for Ox or Red and $\bar{G}_A$ is the minimal free energy of state A. However, simply using this definition does not allow to place the two minima with respect to each other on a free energy diagram. The use of the vertical energy gap as the reaction coordinate leads to a linear dependence between the two free energy curves,[50]

$$G_{\rm Red}(\Delta E) - G_{\rm Ox}(\Delta E) = \Delta E, \tag{8}$$

which enables one to establish a relationship between the origins of the two curves ($\bar{G}_{\rm Red}$ and $\bar{G}_{\rm Ox}$), as well as to use data from the oxidized (reduced) state trajectory to build the free energy profile for the reduced (oxidized) state, *i.e.* in a very low probability region (even beyond the transition state).

Despite this enhanced sampling efficiency, it remains necessary to run long simulations to build the full free energy profiles. This makes the study of ETR with MD rather costly which prevents to carry on systematic studies of the impact of functionalization. Molecular density functional theory (MDFT) is a liquid state theory that we have recently shown to be an efficient alternative[41] to tackle this problem.

C. Molecular Density Functional Theory

We first recall here some basic concepts of MDFT but more detailed descriptions can be found in our previous works[51,52]. MDFT is a flavor of classical density functional theory (cDFT) developed to calculate the solvation free energy of a solute molecule and the equilibrium solvent density surrounding it. The solvent is described by its density field $\rho(\boldsymbol{r},\boldsymbol{\omega})$ which measures the averaged number of solvent molecules with an orientation $\boldsymbol{\omega}$ per unit volume at a given position $\boldsymbol{r}$. The solute molecule interacts with the solvent through an external potential $V_{\rm ext}(\boldsymbol{r},\boldsymbol{\omega})$.

Both solute and solvent are modelled by rigid molecules and therefore there is no intramolecular term in the interaction potential.

According to the cDFT principles, for any external potential, there exists a unique functional of the solvent density that reaches its minimum for the equilibrium solvent density and which is equal to the solvation free energy at this minimum. This functional is split as the sum of three different contributions

$$F[\rho] = F_{\rm ext}[\rho] + F_{\rm id}[\rho] + F_{\rm exc}[\rho]. \tag{9}$$

The first two terms in the right-hand side of Equation 9 are the external and ideal contribution. The first one accounts for the solute-solvent interaction and the second one is the usual entropic term of the ideal gas. There exist exact expressions for those two terms which can be computed with no difficulty[51,52].

The last term is the excess functional, $F_{\rm exc}[\rho]$, which accounts for the solvent-solvent interactions. There is no known exact expression for this term that can be used practically. Approximations are thus required and we will use here the hyper-netted chain (HNC) functional[52] in which $F_{\rm exc}[\rho]$ is expressed as a Taylor expansion truncated at second order around the homogeneous bulk solvent density ρ_b.

D. Modeling electron transfer using MDFT

In this section, we recall some basics of the MDFT framework to study electron transfer reactions. The solvent densities in equilibrium with both redox states and the corresponding solvation free energies can be directly computed by functional minimization of the functional of Equation 4 using the appropriate external potential.

However, exploring densities corresponding to out-of-equilibrium states requires a suitable methodology. We first generate a series of external potentials,

$$V_\eta = (1-\eta)V_{\mathrm{Red}} + \eta V_{\mathrm{Ox}} \tag{10}$$

by linearly interpolating between the external potential generated by the reduced state, V_{Red}, and the one generated by the oxidized state, V_{Ox}. Minimizing the functional of Equation 9 with an external potential V_η generates a solvent density ρ_η. By analogy with Equation 6 we define the averaged vertical energy gap associated to this solvent density

$$\langle \Delta E \rangle_\eta = \iint \rho_\eta(\boldsymbol{r},\boldsymbol{\omega})[V_{\mathrm{Red}}(\boldsymbol{r},\boldsymbol{\omega}) - V_{\mathrm{Ox}}(\boldsymbol{r},\boldsymbol{\omega})]d\boldsymbol{r}d\boldsymbol{\omega} \tag{11}$$

$$= F_{\mathrm{Red}}[\rho_\eta] - F_{\mathrm{Ox}}[\rho_\eta] \tag{12}$$

It should be mentioned that $\langle \Delta E \rangle_\eta$ is the ensemble average of the microscopic VEG of Equation 6 over the phase space associated to V_η. Because there is a one to one mapping between $\langle \Delta E \rangle_\eta$ and ρ_η, the free energy profile of the oxidized state can be computed as a function of this reaction coordinate

$$F_{\mathrm{Red}}(\langle \Delta E \rangle_\eta) \coloneqq F_{\mathrm{Red}}[\rho_\eta]. \tag{13}$$

A dozen of functional minimisation are typically required to build the free energy profiles of a redox couple in a given solvent. The reorganization free energies for the oxidized and reduced states are respectively

$$\lambda_{\mathrm{Red}} = F_{\mathrm{Red}}[\rho_{\mathrm{Ox}}] - F_{\mathrm{Red}}[\rho_{\mathrm{Red}}] \tag{14}$$

$$\lambda_{\mathrm{Ox}} = F_{\mathrm{Ox}}[\rho_{\mathrm{Red}}] - F_{\mathrm{Ox}}[\rho_{\mathrm{Ox}}]. \tag{15}$$

Their computation only requires two functional minimization which is very beneficial when it comes to the investigation of a large amount of solutes.

III. COMPUTATIONAL DETAILS

AIMD simulations were taken from our previous work[38], where the technical details can be found. Classical MD simulations were performed using the MetalWalls code[53] and a recently developed polarizable force field[43]. The simulation cells contain one redox molecule (either AQ or AQ^-) and 95 MeCN molecules. Cubic cells were built using the PACKMOL[54] package. A first run was performed in the NPT ensemble at 298 K and 1 bar to reach the experimental density of MeCN. Then the simulations were carried out in the NVT ensemble at 298 K with cubic cells of 20.55^3 Å^3 for a production time of 50 ns after 1 ns of equilibration. A timestep of 1 fs was used and the trajectory was saved every 500 fs. The equations of motion were integrated using the velocity-Verlet algorithm, and the temperature was kept constant using a chain Nosé-Hoover thermostat[55,56]. The short-range van der Waals interactions were calculated with a cutoff value of 10 Å, while the Ewald summation method was used for electrostatics interactions (involving the partial charges and the induced dipoles).

MDFT calculations are performed with an in-house developed Fortran code. We use a 30^3 Å^3 cubic simulation box with 125 grid nodes in each direction and 66 orientations per grid point. To compute the density and polarisation maps of anthraquinone, a cubic cell of 25^3 Å^3 and 125^3 grid nodes was used to have the same resolution than the maps computed with MD. A 3-sites rigid non-polarizable model is used for MeCN [57]. Preliminary solutes molecular structures were first generated via OpenBabel[58] from the canonical SMILES notation of the molecules. In a second step, we applied the semi-empirical quantum model, Austin model 1, together with the bond charge correction (AM1-BCC)[59,60] to optimise the molecular geometry and to find the atomic charges. Lennard-Jones parameters were taken from the second generation generalised amber force field (gaff2)[61] with a 10 Å cutoff radius. Both AM1-BCC modelling tool and gaff2 force fields database distributed within the AmberTool software package[62] were used. The force field parameters of quinone anions were chosen applying the strategy mentioned in ref.[43]: The structure and the force-field parameters are kept identical to the oxidized form but an excess charge of -0.8 e is evenly split between all non-hydrogen atoms. Note that this excess charge is reduced to -0.8 e to implicitly account for the electronic polarisability as is commonly done in non-polarizable force fields[63,64]. The nondimensional dipolar polarization density can be computed from the equilibrium density

$$\boldsymbol{P}(\boldsymbol{r},\boldsymbol{\omega}) = \iint \rho(\boldsymbol{r},\boldsymbol{\omega})\boldsymbol{\omega}d\boldsymbol{r}d\boldsymbol{\omega}. \tag{16}$$

IV. RESULTS AND DISCUSSION

A. Benchmark of MDFT results with MD simulations

We first look at the solvation structure of AQ solvated in MeCN. The solvent density and the polarization in the plane of the aromatic rings computed with MDFT and classical MD are compared in Figure 2 together with density results obtained using AIMD trajectories. In the case of MD simulations, these quantities were extracted from the trajectories using Travis[65,66] using a sampling volume of $0.2 \times 0.2 \times 4.0$ Å^3, while in MDFT the density is a direct output from the calculation (averaging in a slab of width 4 Å in the z direction was made for comparison purposes).

While the density maps obtained by MD and MDFT displayed in Figure 2 are very similar, it is quite obvious that the AIMD one is undersampled. The AIMD simulation was run for 18 ps with the same box as classical MD, which is a standard simulation time for this method. This illustrates that the high computational cost associated

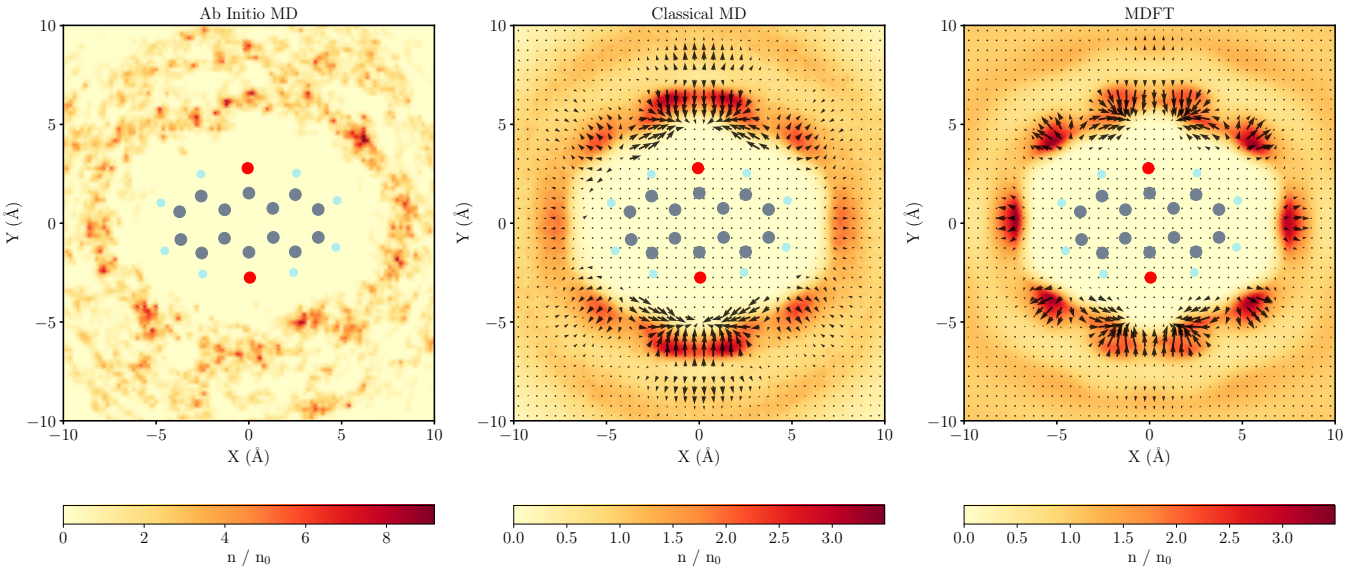

FIG. 2. Two dimensional maps of acetonitrile density and polarization maps in the aromatic plane of anthraquinone computed with *ab-initio* MD, classical MD and MDFT. Grey, blue, and red circles represent carbon, hydrogen, and oxygen atoms, respectively. Polarisation is represented by arrows oriented in the direction of the projection of $\boldsymbol{P}$ and whose length is proportional to $\|\boldsymbol{P}\|$

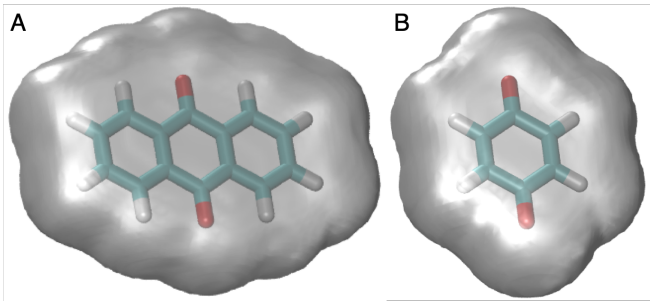

FIG. 3. Solvent density isosurfaces of (A) AQ and (B) BQ at $10^{-2} \times n_0$ calculated by MDFT. Oxygen, hydrogen, and carbon atoms are displayed in red, cyan and white respectively.

with AIMD prevents it to access the 3D structure of the solvent around the solute, this is all the more true for polarization properties which also require a sampling of orientations.

A closer look into the MD and MDFT density maps reveals the existence of two solvation shells, the second one showing few variation in intensity. The first solvation shell is more structured with the presence of ten basins of high density. They are all located in the center of the regions delimited by two vicinal C–H or C=O bonds. The agreement between MDFT and MD is excellent considering the force field used for the acetonitrile solvent and the AQ species differ between the two methods.

We now analyze the polarization density provided by the classical MD and MDFT. On Figure 2 it is represented using vectors, which directions show the projection of the polarization in the plane of the AQ aromatic rings and which lengths are proportional to the intensity of the polarization. To improve the readability of the figure, orientations are depicted on a grid 2.5 times looser than the one used for calculation. Again, a very good agreement is found between classical MD and MDFT for the prediction of the polarization maps. In the first solvation shell, MeCN dipoles point towards the oxygen of the carbonyl groups and outwards the solute around the C–H bonds. This is an expected behaviour: the negatively charged oxygen atoms attract the positively charged CH_3 fragment of the solvent molecule while the positively charged hydrogen atoms attract the negatively charged nitrile fragment. Between C–H bonds and the carbonyl groups, MeCN dipoles lie almost parallel to the cavity surface created by AQ as shown in Figure 3A. This cavity surface is defined as the isosurface on which the solvent density is at $10^{-2} \times n_0$ where n_0 is the bulk density. The value of the polarization is considerably reduced in the second solvation shell because the electric field generated by the solute is screened by the first solvation shell. The vectors are antialigned with the polarization observed in the first solvation shell. This comparison proves that MDFT is able to predict faithfully the structural properties of solvation around AQ. This is of great interest because MDFT is far less computationally demanding: it took more than 100 hours on a 44 core skylake computer to run the 50 ns MD trajectory that was used to compute the density and polarization maps displayed in Figure 2B while the MDFT calculation to compute the maps displayed in Figure 2C took less than 6 minutes on the same computer.

We now turn to the energetic properties for the electron

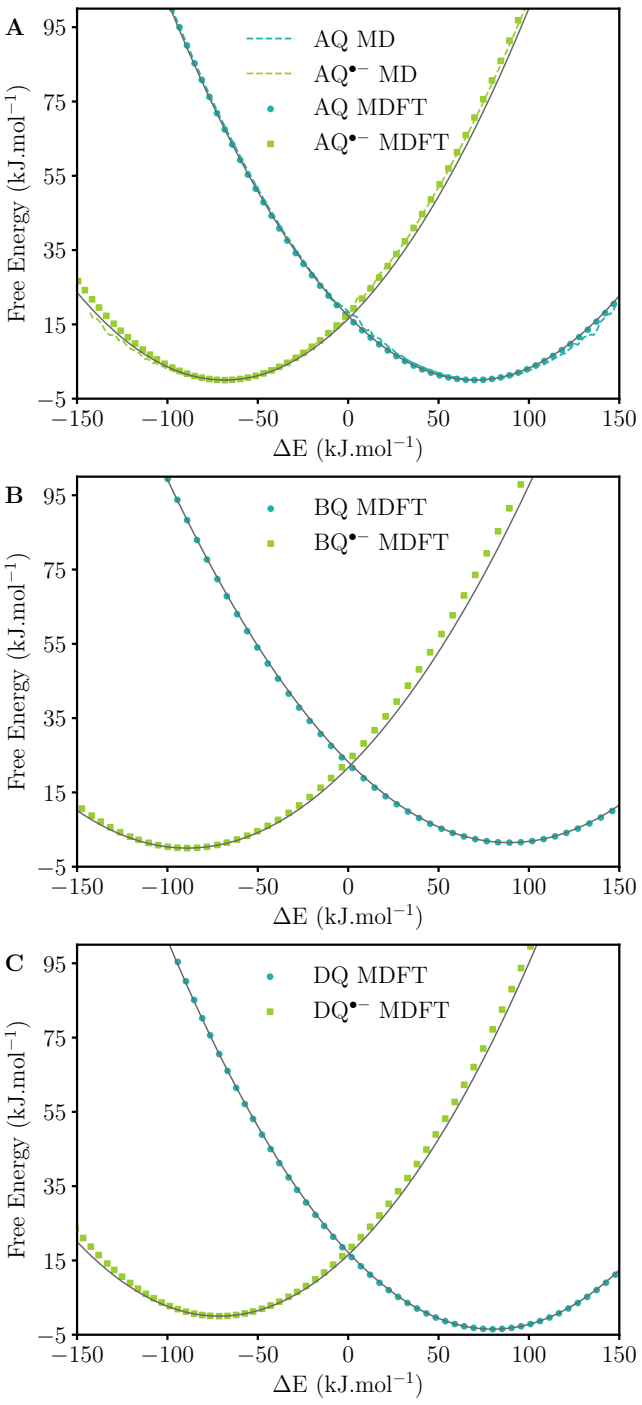

FIG. 4. Free energy profiles of electron transfer half reactions of (A) AQ and AQ^- calculated by classical MD and MDFT, (B) BQ and BQ^-, (C) DQ and DQ^- calculated by MDFT. As described in the text, the vertical energy gaps were shifted by the same constant value, which was chosen in order to align the minima for the AQ/AQ^- redox couple. Solid lines are fit of MDFT results using Marcus theory.

transfer half-reaction. We first examine the redox half reaction between AQ and AQ^- solvated in MeCN. Free energy profiles of the two species are computed with classical MD using the procedure described in Section II B. The same reaction is studied with MDFT where we generated a series of potential V_η by varying η in Equation 10 between -0.3 and 1.3 by increment of 1/30. Using values of $\eta > 1$ and $\eta < 0$ allows to compute the branches of the free energy profiles in regions corresponding to the left hand-sign of the negative minimum (reduced state) and right hand side of the positive minimum (oxidized state).

As mentioned above, the estimation of the free energy curves from MD allows to calculate the free energy difference between the two states – the same argument also applies to MDFT. However, this free energy difference cannot readily be compared to experimentally measured potentials unless it can be calibrated with another chemical reaction[67]. This was made in the case of AIMD by setting up a computational standard hydrogen electrode[6] and more recently a computational Ag/AgCl reference electrode[68]. In the present work, the use of classical methods prevents us from building such absolute scales, so that we use the AQ/AQ^- as a reference. In practice, this is made by assigning an arbitrary energy constant to the free electron in Equation 1 so that the minima of the free energy profiles align for this couple – the same shift is then used for all the other couples. Yet it is not possible to comment these free energy differences with respect to experimental values since our calculations do not include the dominant intramolecular energy term, which is properly taken into account in quantum chemistry calculations[2,20]. In this work we therefore focus on the value of the solvent reorganization free energy. Note that applying a shift to the VEG values has no influence on this quantity. Moreover, because we concomitantly shift the ensemble averaged VEG defined in Equation 7, the crossing point of the two curves is still at $< \Delta E >_\eta = 0$ as it should be by the definition in Equation 7.

The free energy profiles obtained for the AQ/AQ^- couple using MD and MDFT are compared on Figure 4A. Overall, the agreement is excellent both for the curvatures and the position of the minima. To check if this half reaction can be described with Marcus theory we computed the reorganization free energy of AQ and AQ^- with Equation 14. MD gives a value of 72.3 kJ/mol for both states while MDFT predicts the reorganization free energies of 66.8 and 69.3 kJ/mol for AQ and AQ^-, respectively. The values of the reorganization free energies differ by less than 5 % between the two states which implies that this system can be described with a very good approximation using Marcus Theory. Thus, we have fitted the MDFT data using two parabolas with the same curvature (and hence a single λ), as depicted in Figure 4.

To further test our methodology, we computed the free energy profiles of the electron transfer involved in the benzoquinone (BQ) and duroquinone (DQ) redox couples solvated in MeCN since these systems were already studied using an *ab initio*-based approach by VandeVondele

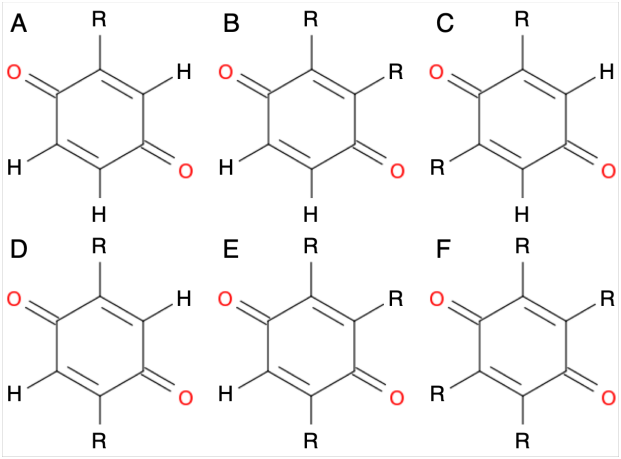

FIG. 5. Primary molecular structure of (A) 2-BQ, (B) 2,3-BQ, (C) 2,6-BQ, (D) 2,5-BQ, (E) 2,3,5-BQ, and (F) 2,3,5,6-BQ derivatives. R's represent the sites to be substituted by functional groups.

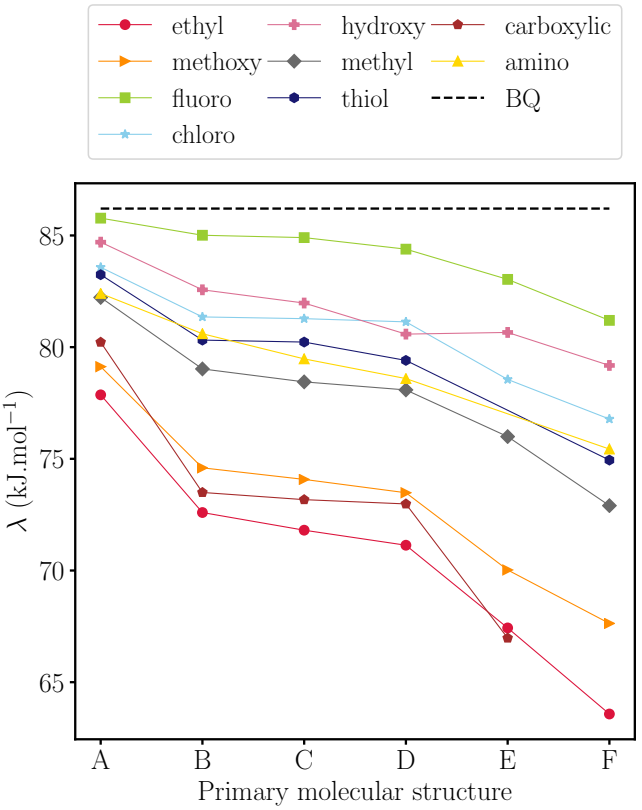

FIG. 6. Solvent reorganization free energies of functionalized BQ derivatives as a function of substitution positions. The notation of primary molecular structures follows those in Figure 5. The black dashed line is the reorganization free energy of BQ.

et al.[37]. The free energy profiles are respectively plotted in Figure 4B and 4C. For these redox couples as well, they are well fitted by pairs of parabolas with identical curvature indicating that those 2 ETR are well described by Marcus theory. The reorganization free energies obtained using MDFT are 86.8 kJ/mol for BQ/ BQ^-, and 74.0 kJ/mol/DQ and DQ^-. They are in good agreement with the DFT simulations[37], from which values of 78.3 and 69.4 kJ/mol were reported for BQ and DQ, respectively. A qualitative agreement is obtained even if the MDFT results are overestimated by about 10 % with respect to the AIMD results.

B. Electron transfer of Benzoquinone derivatives

We now take advantage of the computational efficiency of MDFT to carry on an extensive study of the impact of functionalization on the electron transfer properties of quinones. More precisely, we determine the effect of chemical substitutions by studying the six derivatives of BQ displayed on Figure 5. These are obtained by systematically substituting the H atoms with a functional group. For simplicity, we only consider BQ derivatives substituted with a single type of functional group. The chemical functions considered in this work are methyl (–CH_3), ethyl (–CH_2CH_3), methoxy (–OCH_3), amino (–NH_2), hydroxy (–OH), fluoro (–F), chloro (–Cl), thiol (–SH), and carboxyl (–COOH).

We first calculate the reorganization free energies of the oxidized and reduced states. As for the benchmark molecules, they differ by less than 5 % for the whole set of molecules so that all the redox couples can be considered as being well described by Marcus theory and attributed a single λ value. The corresponding reorganization free energies are displayed on Figure 6. Firstly, we notice that all the functionalized BQ have a reorganization free energy lower than that of the parent molecule. There is also a clear trend of the evolution of the reorganization free energy with the number of functional groups: the more the molecule is functionalized the lower is the reorganization free energy. Finally, there is little difference between the different di-functional quinones, but we can see that molecules where the functional groups are in positions 2 and 3 have the highest λ, while molecules where the functional group are in positions 2 and 5 have the lowest one. Regarding the influence of the functional group, sorting them from the highest to lowest reorganization free energy we obtain the global trend: –F > –OH > –Cl > –SH > $–NH_2$ > $–CH_3$ > $–OCH_3$ > –COOH > $–CH_2CH_3$.

In an attempt to rationalize this behaviour we estimated the volume of each functional group as the difference of cavity volume between the monofunctionalized BQ and BQ. Cavity volume is defined as the volume of the space where the solvent density is below $10^{-2} \times n_0$. Examples of such volumes for AQ and BQ are displayed on Figure 3. The variation of λ with respect to the volume of functional groups is displayed in the bottom panel of Figure 7. A strong correlation between the two quantities is observed for the whole range of functional groups, with the excep-

tion of the amino one. Recalling that the activation free energy, and thus the rate constant of ETR, is connected to the activation free energy this could be a way to fine tune the kinetics of the ETR. However, we emphasize that this approach cannot capture the full picture of the ETR since internal reorganization of the solute, in particular due to electronic effects, is neglected. The latter may be important in the case of complex chemical entities and affect the kinetics aspect as well.

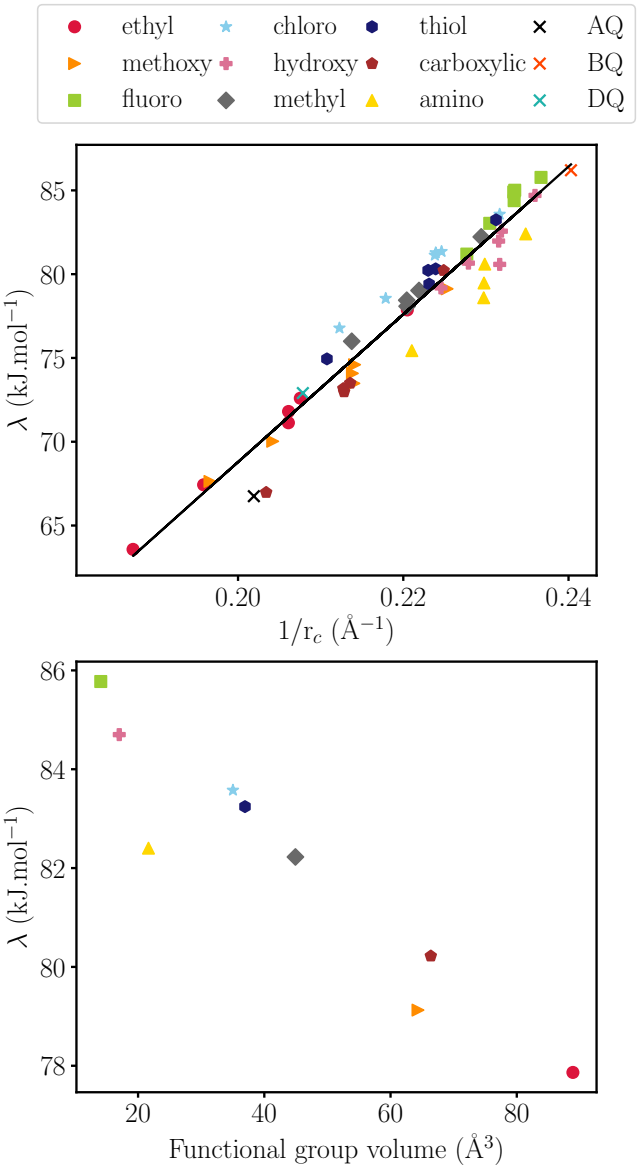

FIG. 7. Top: Solvent reorganization free energies of AQ, BQ and BQ derivatives with respect to the inverse cavity radius, $1/r_c$. The solid line is a linear regression of the data. Bottom: Solvent reorganization free energies of mono-functionalized BQ derivatives with respect to the volume of the functional group estimated as the difference of cavity volume between the mono-functionalized BQ and BQ.

Since we have access to the reorganization free energies and the solvation structure for the full set of functionalized molecules, we finally test the relation 5 that links λ to the solute radius. This is a difficult test since this relation was derived for spherical solutes, which is clearly not the case here as evidenced by the molecular structure displayed in Figure 5 and by the solvent density isosurface around BQ and AQ displayed in Figure 3. To do so, we define the cavity radius r_c as the radius of a sphere of identical volume to the cavity created by the solute. The reorganization free energy is plotted as a function of the inverse of the cavity radius on the top panel of Figure 7. The linear relationship between λ et $1/r_c$ is well verified overall. A linear regression of the data excluding AQ that has a different aromatic structure gives a slope of 440 kJ Å mol^{-1}. The theoretical value, calculated by inserting $\epsilon_{op} = 1$ (because molecules are assumed to be rigid) and $\epsilon_s = 31.6$ for the solvent[57] into Equation 5, is 673 kJ Å mol^{-1}. Such a difference is not surprising considering the non-sphericity of the solute. If we take a closer look into the difference between functional groups, we can see that carboxylic, amino, methoxy and hydroxy groups lead to λ values slightly below the linear regression yet chloro and fluoro groups have a reverse effect. Functional group with larger dipole moment are thus lying below the linear regression. However, this effect remains weak compared to the general trend with respect to the molecular radius.

V. CONCLUSIONS

In this work we carry a systematic study of the influence of functionalization on the reorganization free energies of benzoquinone derivatives. We first validate our methodology by carrying on a detailed comparison of the solvent structural properties around AQ predicted using MDFT and classical MD. The force fields used in the two methods differ since (i) molecules are rigid in MDFT while they are flexible in MD (ii) the solvent model is coarse grained in MDFT while it is all-atom in MD. Despite these differences the agreement between the two approaches is very satisfactory. The density peaks in the first solvation shell are well reproduced, and more importantly the polarization maps are highly similar indicating that the solvent orientation properties are also well captured by MDFT. The agreement between the two methods is not limited to the solvation structure since the free energy profiles computed for both redox states with MD and MDFT are almost identical. We found that the AQ/AQ$^-$ electron transfer half-reaction is in good agreement with Marcus prediction since the two species free energy profiles are well fitted by parabolas of identical curvature. This establishes MDFT as an appropriate method to study the ETR of quinone derivatives while it requires 10^3 less computational times than MD to study the same system. To be fair, using a non-polarizable force field in MD would reduce the computational cost by one order of magnitude, but the gap would remain very large.

This computational efficiency allows to systematically study the influence of functionalization on the reorganization free energy of electron transfer half reaction involving BQ derivatives. Here again, we found that the whole set of molecules considered in this study follows Marcus picture with identical values for the reorganization free energies of the oxidized and reduced states. The values of the reorganization free energy of each functionalized molecule is lower than the value for the non-functionalized parent BQ. The more the molecule is functionalized, the lower is its solvation free energy. Finally, we found a correlation between the value of the reorganization free energy and the volume of the functional group. This lead us to check the linear scaling of the reorganization free energy with the inverse of the cavity radius. This relation is indeed verified but with a slope that differs from the theoretical values, the difference being attributed to the non sphericity of the cavity created by the solute.

Overall, this work shows that MDFT is a suitable method to account for the functional effects on the solvent reorganization free energies of electron transfer reaction. In the future, systematic studies could thus be performed in order to understand the rate constant of the redox reactions. Of course having a full picture of the reactions free energy profile would require to account for internal degrees of freedom using electronic structure methods. A promising approach to fully address this problem could be the QM/MDFT hybrid approach one of us recently proposed[69]. In this approach the solute is dealt with at the quantum level using electronic DFT while the solvent degrees of freedom are accounted at the classical level using MDFT. We believe that this method could be the appropriate compromise between precision and computational cost to make the calculation of ETR rate constant in solution feasible in the future.

VI. ACKNOWLEDGEMENT

This project has received funding from the European Research Council (ERC) under the European Union's Horizon 2020 research and innovation programme (grant agreement No. 771294). This work was granted access to the HPC resources of IDRIS under Allocation A0120910463 made by GENCI. We acknowledge support from EoCoE, a project funded by the European Union Contract No. H2020-INFRAEDI-2018-824158. The authors thank the French National Research Agency (STORE-EX Labex Project ANR-10-LABX-76-01) for financial support..

[1] J. Yu, T.-S. Zhao, and D. Pan, J. Phys. Chem. Lett. **11**, 10433 (2020).
[2] M. T. Huynh, C. W. Anson, A. C. Cavell, S. S. Stahl, and S. Hammes-Schiffer, J. Am. Chem. Soc. **138**, 15903 (2016).
[3] M. S. Graige, M. L. Paddock, J. M. Bruce, G. Feher, and M. Y. Okamura, J. Am. Chem. Soc. **118**, 9005 (1996).
[4] M. A. Bhat, Electrochim. Acta **81**, 275 (2012).
[5] M. Quan, D. Sanchez, M. F. Wasylkiw, and D. K. Smith, J. Am. Chem. Soc. **129**, 12847 (2007).
[6] J. Cheng, M. Sulpizi, and M. Sprik, J. Chem. Phys. **131**, 154504 (2009).
[7] M. Liu and S. Lu, Front. Plant Sci. **7**, 1898 (2016).
[8] H. Kurreck and M. Huber, Angew. Chem. Int. Ed. **34**, 849 (1995).
[9] P. Mitchell, J. Theor. Biol. **62**, 327 (1976).
[10] B. Søballe and R. K. Poole, Microbiology **145**, 1817 (1999).
[11] C. Han, H. Li, R. Shi, T. Zhang, J. Tong, J. Li, and B. Li, J. Mater. Chem. A **7**, 23378 (2019).
[12] Y. Ding, C. Zhang, L. Zhang, Y. Zhou, and G. Yu, Chem. Soc. Rev. **47**, 69 (2018).
[13] B. Yang, L. Hoober-Burkhardt, F. Wang, G. K. S. Prakash, and S. R. Narayanan, J. Electrochem. Soc. **161**, A1371 (2014).
[14] P. Leung, T. Martin, Q. Xu, C. Flox, M. Mohamad, J. Palma, A. Rodchanarowan, X. Zhu, W. Xing, and A. Shah, Appl. Energy **282**, 116058 (2021).
[15] E. Mourad, L. Coustan, P. Lannelongue, D. Zigah, A. Mehdi, A. Vioux, S. Freunberger, F. Favier, and O. Fontaine, Nat. Mater. **16**, 446 (2017).
[16] K. Lin, Q. Chen, M. R. Gerhardt, L. Tong, S. B. Kim, L. Eisenach, A. W. Valle, D. Hardee, R. G. Gordon, M. J. Aziz, and M. P. Marshak, Science **349**, 1529 (2015).
[17] B. Huskinson, M. P. Marshak, C. Suh, S. Er, M. R. Gerhardt, C. J. Galvin, X. Chen, A. Aspuru-Guzik, R. G. Gordon, and M. J. Aziz, Nature **505**, 195 (2014).
[18] E. J. Son, J. H. Kim, K. Kim, and C. B. Park, J. Mater. Chem. A **4**, 11179 (2016).
[19] R. P. Fornari and P. de Silva, Wiley Interdiscip. Rev. Comput. Mol. Sci. **11**, e1495 (2021).
[20] S. Er, C. Suh, M. P. Marshak, and A. Aspuru-Guzik, Chem. Sci. **6**, 885 (2015).
[21] K. Wedege, E. Dražević, D. Konya, and A. Bentien, Sci. Rep. **6**, 39101 (2016).
[22] D. P. Tabor, R. Gómez-Bombarelli, L. Tong, R. G. Gordon, M. J. Aziz, and A. Aspuru-Guzik, J. Mater. Chem. A **7**, 12833 (2019).
[23] S. D. Pineda Flores, G. C. Martin-Noble, R. L. Phillips, and J. Schrier, J. Phys. Chem. C **119**, 21800 (2015).
[24] Y. Jing, E. M. Fell, M. Wu, S. Jin, Y. Ji, D. A. Pollack, Z. Tang, D. Ding, M. Bahari, M.-A. Goulet, T. Tsukamoto, R. G. Gordon, and M. J. Aziz, ACS Energy Lett. **7**, 226 (2022).
[25] N. V. Rees, A. D. Clegg, O. V. Klymenko, B. A. Coles, and R. G. Compton, J. Phys. Chem. B **108**, 13047 (2004).
[26] M. Zamadar, A. R. Cook, A. Lewandowska-Andralojc, R. Holroyd, Y. Jiang, J. Bikalis, and J. R. Miller, J. Phys. Chem. A **117**, 8360 (2013).
[27] S. R. Belding, J. G. Limon-Petersen, E. J. F. Dickinson, and R. G. Compton, Angew. Chem. Int. Ed. **49**, 9242 (2010).
[28] R. A. Marcus, J. Chem. Phys. **24**, 966 (1956).
[29] R. A. Marcus, J. Chem. Phys. **24**, 979 (1956).
[30] R. A. Marcus, J. Chem. Phys. **26**, 867 (1957).
[31] R. A. Marcus, J. Chem. Phys. **26**, 872 (1957).
[32] R. A. Marcus, Discuss. Faraday Soc. **29**, 21 (1960).
[33] R. A. Marcus, J. Chem. Phys. **38**, 1858 (1963).
[34] R. A. Marcus, J. Phys. Chem. **67**, 853 (1963).
[35] R. A. Marcus, J. Chem. Phys. **43**, 679 (1965).
[36] R. A. Marcus, J. Electroanal. Chem. Electron Transfer in Protein and Supramolecular Assemblies at Interfaces, **438**, 251 (1997).
[37] J. VandeVondele, M. Sulpizi, and M. Sprik, Angew. Chem. Int. Ed. **45**, 1936 (2006).
[38] K. G. Reeves, A. Serva, G. Jeanmairet, and M. Salanne, Phys. Chem. Chem. Phys. **22**, 10561 (2020).
[39] S.-J. Yang, X.-Y. Qin, R. He, W. Shen, M. Li, and L.-B. Zhao, Phys. Chem. Chem. Phys. **19**, 12480 (2017).
[40] R. Vuilleumier, K. A. Tay, G. Jeanmairet, D. Borgis, and A. Boutin, J. Am. Chem. Soc. **134**, 2067 (2012).
[41] G. Jeanmairet, B. Rotenberg, M. Levesque, D. Borgis, and M. Salanne, Chem. Sci. **10**, 2130 (2019).
[42] T.-Y. Hsu and G. Jeanmairet, J. Chem. Phys. **154**, 131102 (2021).
[43] R. Berthin, A. Serva, K. G. Reeves, E. Heid, C. Schröder, and M. Salanne, J. Chem. Phys. **155**, 074504 (2021).
[44] R. M. Lynden-Bell, Electrochem. commun. **9**, 1857 (2007).

[45]M. J. Weaver, in *Comprehensive Chemical Kinetics*, Vol. 27 (Elsevier, 1988) pp. 1–60.
[46]W. R. Fawcett and M. Opallo, Angew. Chem. Int. Ed. **33**, 2131 (1994).
[47]N. Sutin, in *Progress in Inorganic Chemistry*, edited by S. J. Lippard (John Wiley & Sons, Inc., 2007) pp. 441–498.
[48]D. H. Evans, Chem. Rev. **108**, 2113 (2008).
[49]A. Warshel, J. Phys. Chem. **86**, 2218 (1982).
[50]J. Blumberger and M. Sprik, in *Computer Simulations in Condensed Matter Systems: From Materials to Chemical Biology Volume 2*, Lecture Notes in Physics, edited by M. Ferrario, G. Ciccotti, and K. Binder (Springer Berlin Heidelberg, 2006) pp. 481–506.
[51]G. Jeanmairet, M. Levesque, R. Vuilleumier, and D. Borgis, J. Phys. Chem. Lett. **4**, 619 (2013).
[52]L. Ding, M. Levesque, D. Borgis, and L. Belloni, J. Chem. Phys. **147**, 094107 (2017).
[53]A. Marin-Laflèche, M. Haefele, L. Scalfi, A. Coretti, T. Dufils, G. Jeanmairet, S. K. Reed, A. Serva, R. Berthin, C. Bacon, S. Bonella, B. Rotenberg, P. A. Madden, and M. Salanne, J. Open Source Softw. **5**, 2373 (2020).
[54]L. Martínez, R. Andrade, E. G. Birgin, and J. M. Martínez, J. Comput. Chem. **30**, 2157 (2009).
[55]S. Nosé, J. Chem. Phys. **81**, 511 (1984).
[56]D. J. Evans and B. L. Holian, J. Chem. Phys. **83**, 4069 (1985).
[57]D. M. Edwards, P. A. Madden, and I. R. McDonald, Mol. Phys. **51**, 1141 (1984).
[58]N. M. O'Boyle, M. Banck, C. A. James, C. Morley, T. Vandermeersch, and G. R. Hutchison, J. Cheminform. **3**, 33 (2011).
[59]A. Jakalian, B. L. Bush, D. B. Jack, and C. I. Bayly, J. Comput. Chem. **21**, 132 (2000).
[60]A. Jakalian, D. B. Jack, and C. I. Bayly, J. Comput. Chem. **23**, 1623 (2002).
[61]J. Wang, R. M. Wolf, J. W. Caldwell, P. A. Kollman, and D. A. Case, J. Comput. Chem. **25**, 1157 (2004).
[62]D. Case, H. Aktulga, K. Belfon, I. Ben-Shalom, S. Brozell, D. Cerutti, I. T.E. Cheatham, G. Cisneros, V. Cruzeiro, T. Darden, R. Duke, G. Giambasu, M. Gilson, H. Gohlke, A. Goetz, R. Harris, S. Izadi, S. Izmailov, C. Jin, K. Kasavajhala, M. Kaymak, E. King, A. Kovalenko, T. Kurtzman, T. Lee, S. LeGrand, P. Li, C. Lin, J. Liu, T. Luchko, R. Luo, M. Machado, V. Man, M. Manathunga, K. Merz, Y. Miao, O. Mikhailovskii, G. Monard, H. Nguyen, K. O'Hearn, A. Onufriev, F. Pan, S. Pantano, R. Qi, A. Rahnamoun, D. Roe, A. Roitberg, C. Sagui, S. Schott-Verdugo, J. Shen, C. Simmerling, N. Skrynnikov, J. Smith, J. Swails, R. Walker, J. Wang, H. Wei, R. Wolf, X. Wu, Y. Xue, D. York, S. Zhao, and P. Kollman, University of California, San Francisco (2021).
[63]I. Leontyev and A. Stuchebrukhov, Phys. Chem. Chem. Phys. **13**, 2613 (2011).
[64]B. J. Kirby and P. Jungwirth, J. Phys. Chem. Lett. **10**, 7531 (2019).
[65]M. Brehm and B. Kirchner, J. Chem. Inf. Model. **51**, 2007 (2011).
[66]M. Brehm, M. Thomas, S. Gehrke, and B. Kirchner, J. Chem. Phys. **152**, 164105 (2020).
[67]J. Cheng and M. Sprik, Phys. Chem. Chem. Phys. **14**, 11245 (2012).
[68]X.-H. Yang, A. Cuesta, and J. Cheng, J. Phys. Chem. B **123**, 10224 (2019).
[69]G. Jeanmairet, M. Levesque, and D. Borgis, J. Chem. Theory Comput. **16**, 7123 (2020).